JACS
JOURNAL OF THE AMERICAN CHEMICAL SOCIETY

pubs.acs.org/JACS

Article

Quantitative Electro-Reduction of CO_2 to Liquid Fuel over Electro-Synthesized Metal–Organic Frameworks

Xinchen Kang, Bin Wang, Kui Hu, Kai Lyu, Xue Han, Ben F. Spencer, Mark D. Frogley, Floriana Tuna, Eric J. L. McInnes, Robert A. W. Dryfe, Buxing Han,* Sihai Yang,* and Martin Schröder*

Cite This: *J. Am. Chem. Soc.* 2020, 142, 17384–17392

Read Online

ACCESS | Metrics & More | Article Recommendations | Supporting Information

ABSTRACT: Efficient electro-reduction of CO_2 over metal–organic framework (MOF) materials is hindered by the poor contact between thermally synthesized MOF particles and the electrode surface, which leads to low Faradaic efficiency for a given product and poor electrochemical stability of the catalyst. We report a MOF-based electrode prepared via electro-synthesis of MFM-300(In) on an indium foil, and its activity for the electrochemical reduction of CO_2 is assessed. The resultant MFM-300(In)-e/In electrode shows a 1 order of magnitude improvement in conductivity compared with that for MFM-300(In)/carbon-paper electrodes. MFM-300(In)-e/In exhibits a current density of 46.1 mA cm^{-2} at an applied potential of −2.15 V vs Ag/Ag^+ for the electro-reduction of CO_2 in organic electrolyte, achieving an exceptional Faradaic efficiency of 99.1% for the formation of formic acid. The facile preparation of the MFM-300(In)-e/In electrode, coupled with its excellent electrochemical stability, provides a new pathway to develop efficient electro-catalysts for CO_2 reduction.

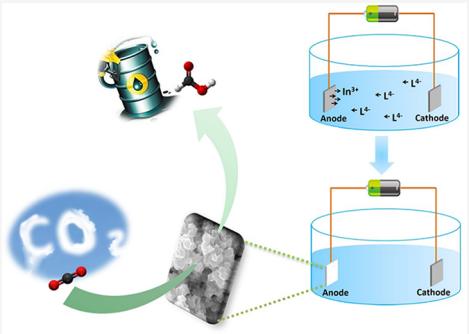

INTRODUCTION

Efficient conversion of CO_2 into chemical feedstocks and fuels is a highly desirable but extremely challenging target.[1−3] Reduction of CO_2 into useful chemicals via thermo-catalysis and photocatalysis has been studied very widely.[4−7] However, the former often requires both high temperature and pressure to activate CO_2, while the latter relies heavily upon the use of sacrificial agents, typically organic amines, thus limiting long-term applications. Electro-catalysis enables the storage of intermittent renewable energy into chemical energy,[8−10] and there are powerful drivers for the development of active, selective and stable electro-catalysts for the efficient reduction of anthropogenic CO_2 emission via conversion to valuable chemicals.[11−14] Electrocatalytic reduction of CO_2 normally relies upon the use of active transition metals (e.g., Cu, Co, and Pd) to reduce the high overpotentials required to activate CO_2 to the $CO_2^{\bullet-}$ radical anion or other intermediates that can be converted further.[15−17]

Metal–organic frameworks (MOFs) are crystalline hybrid materials constructed from metal ions or clusters bridged by polydentate organic ligands.[18−20] Compared with conventional electro-catalysts, MOFs have unique features for the electrochemical reduction of CO_2.[21,22] Metal sites (e.g., Co, Cu, Fe, and Ni) that show activity for CO_2 electro-reduction[23−26] can be readily incorporated into MOF structures via single-site dispersion. Additionally, the intrinsic and tunable porosity of MOFs can lead to high capacity adsorption and selectivity to CO_2,[27,28] thus promoting activation and further conversion. Gaseous products obtained from electro-reduction of CO_2 (e.g., CO and CH_4) often show lower adsorption in MOFs than CO_2 and can thus be readily recovered and the MOF electrode regenerated.[21] MOFs have inherent design flexibility via choice of metal ions and organic ligands, and therefore, their function and activity for electro-reduction of CO_2 can be optimized.[29]

To date, universal approaches to fabricate efficient MOF-based electrodes showing high charge-transfer capacity have been rarely reported.[30−33] Normal methods are based upon the doping of MOF materials onto an electrode substrate.[34] Although various electrodes loaded with MOFs have been studied for the electro-reduction of CO_2, the poor contact between the catalyst and substrate surface limits their performance.[21] Indium-based materials have demonstrated excellent performance for the electro-reduction of CO_2.[35,36] Although electrodeposition of MOFs, particularly Cu- and Zn-based systems, has been described,[37−40] the electro-synthesis of In-based MOFs has not been reported previously. We therefore sought to develop an In electrode decorated with a MOF film that might incorporate active defect sites and show high charge transfer capacity.

Received: May 31, 2020
Published: September 30, 2020

https://dx.doi.org/10.1021/jacs.0c05913
J. Am. Chem. Soc. 2020, 142, 17384–17392

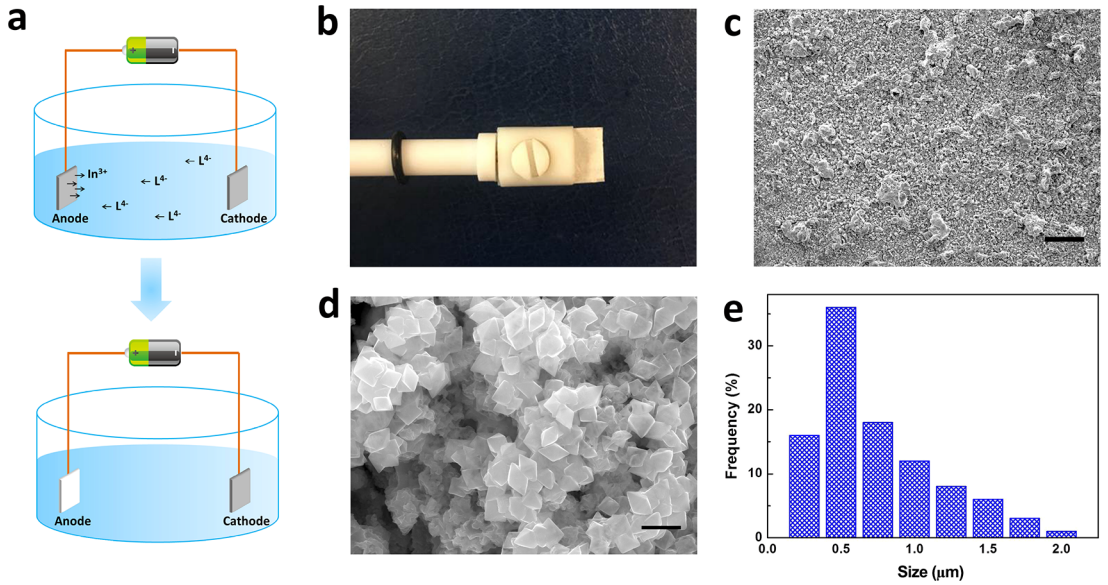

Figure 1. (a) Schematic diagram for the electro-synthesis of MFM-300(In)-e. (b) Photograph of the as-synthesized MFM-300(In)-e on indium foil (0.5 × 1 cm^2). (c and d) SEM images for MFM-300(In)-e. (e) Particle size distribution of MFM-300(In)-e. The scale bars of panels c and d are 200 and 2 μm, respectively.

Here, we report a facile route to the fabrication of such decorated electrodes via electro-synthesis of MOFs onto a metal foil substrate. The MFM-300(In)-e/In electrode ("e" is short for electro-synthesis) prepared in this way shows a 1 order of magnitude enhancement in electrical conductivity compared with electrodes prepared using MOFs prepared by thermo-chemical methods. More importantly, exceptional activities for the electro-reduction of CO_2 are observed with a current density of 46.1 mA cm^{-2} under an applied potential of −2.15 V vs Ag/Ag^+. A Faradaic efficiency of 99.1% for formic acid after 2 h of electrolysis is observed. We also found that the electro-synthesized MOF incorporates structural defects in the form of additional framework In^{3+} sites, which, coupled with improved charge transfer capacity, greatly promote the activation of CO_2 to the radicals, consistent with the observed excellent electrocatalytic activity and stability of the catalyst. Density functional theory (DFT) calculations are applied to reveal the mechanism of catalysis.

RESULTS AND DISCUSSION

Materials Preparation and Characterizations. Samples of MFM-300(In)-t ("t" is short for thermo-synthesis) were obtained by solvothermal reaction of $In(NO_3)_3{\cdot}5H_2O$ and biphenyl-3,3′,5,5′-tetracarboxylic acid (H_4L; Figure S1) in a mixture of DMF and MeCN at 85 °C for 3 days.[41] The crystal structure of MFM-300(In) is shown in Figure S2. The electro-synthesis of MFM-300(In)-e was achieved using indium foil (In-foil) as both the cathode and anode in a solvent mixture of DMF/dioxane/water containing H_4L with 1-ethyl-3-methyl-imidazolium acetate (EmimOAc, structure shown in Figure S3) as the supporting electrolyte (Figure 1a). The formation of MOF occurred rapidly at an applied potential of 10 V and 60 °C, and the In-foil anode was covered by particles of MFM-300(In)-e within 200 s (Figure 1b). The electro-synthesis was then terminated as the surface of In-foil became fully covered with MOF particles thus limiting the supply of further In^{3+} ions from the anode for MOF synthesis. No MOF particle was detected in the electrolyte, indicating that particles of MFM-300(In)-e have a strong interaction with the In-foil substrate. The MFM-300(In)-e/In electrode was then immersed in acetone for 2 h and dried before being used as the MFM-300(In)-e/In electrode. Scanning electron microscopy confirms that the In-foil metal surface is coated uniformly with MFM-300(In)-e, which has an octahedral morphology with a narrow particle size distribution centered at ∼500 nm (Figures 1c−e). By comparison, MFM-300(In)-t shows cube-shaped crystals with an average particle size of ∼2.5 μm (Figure S4). These differences in morphology result only in small differences in the relative intensity of powder X-ray diffraction (PXRD) peaks for MFM-300(In)-t and MFM-300(In)-e (Figure 2a).

Powder crystalline samples of MFM-300(In)-e were carefully scraped off the In-foil for characterisations. The crystal structure and phase purity of MFM-300(In)-e were confirmed by PXRD (Figure 2a); the increased peak width of MFM-300(In)-e compared with MFM-300(In)-t is consistent with their particle size distributions. Full chemical analysis suggests that the indium contents are 35.3 and 32.5 wt % in MFM-300(In)-e and MFM-300(In)-t, respectively. Negligible N content was detected in MFM-300(In)-e, indicating that the ionic liquid cations were removed completely during the solvent exchange process. The higher content of In^{3+} in MFM-300(In)-e suggests that acetate anions OAc^- introduced in the synthesis with EmimOAc are bound to the framework to balance the charge. The slightly higher residual solid observed in the thermogravimetric analysis (TGA) is consistent with the presence of additional In^{3+} in the framework of MFM-300(In)-e (Figure S5), while the slightly lower stability of MFM-300(In)-e compared with MFM-300(In)-t originates most likely from defects in the framework structure. The band observed near 1550 cm^{-1} by Fourier-transform infrared (FTIR) spectroscopy is assigned to the vibration of the carboxylate group, but has an apparent red shift (20 cm^{-1}) for MFM-300(In)-e (Figure 2b), consistent with the presence of some coordinated acetate in this material. The Brunauer−Emmett−Teller (BET) surface areas of MFM-300(In)-t and MFM-300(In)-e are determined to be 1043 and 863 m^2 g^{-1},

https://dx.doi.org/10.1021/jacs.0c05913
J. Am. Chem. Soc. 2020, 142, 17384−17392

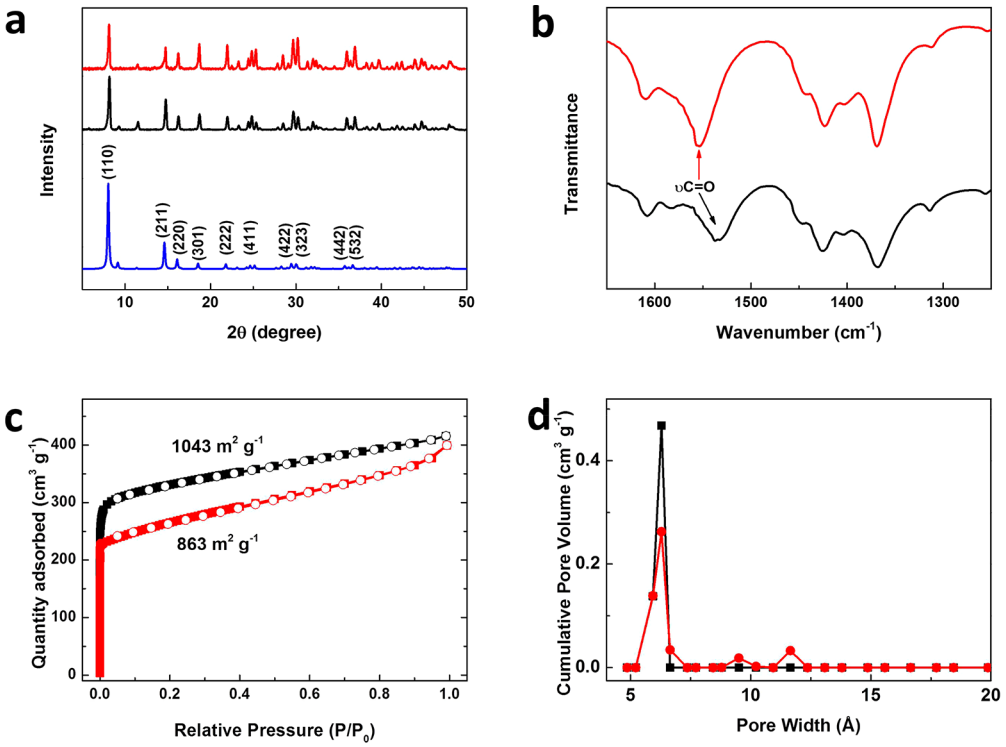

Figure 2. Characterization of as-synthesized MFM-300(In)-t (black line) and MFM-300(In)-e (red line). (a) PXRD patterns. (b) FTIR spectra. (c) N_2 adsorption/desorption isotherms at 77 K. (d) Pore size distribution derived from NLDFT calculations.

respectively (Figure 2c). The slightly reduced surface area of MFM-300(In)-e is attributed to the partial collapse of micropores during the rapid electro-synthesis. Pore size distributions of MFM-300(In)-t and MFM-300(In)-e estimated by nonlocal density functional theory (NLDFT) calculations (Figure 2d) confirm a micropore profile centered at 6.5 Å. In addition, there are two small peaks centered at 9.5 and 11.5 Å in MFM-300(In)-e owing to the presence of defects in the framework. During the electro-synthesis, we propose that the In-foil is oxidized to In^{3+} which binds OAc^- anions from the EmimOAc electrolyte at the surface of the electrode thus preventing full dissolution of In^{3+}. Binding of the tetracarboxylate ligand to In^{3+} occurs at the surface either directly or via replacement of OAc^- to assemble the framework structure uniformly across the In-foil surface.[42] Since there are abundant In^{3+} ions at and around the anode, the as-synthesized MFM-300(In)-e contains excess In^{3+} sites with some associated OAc^-. Both MFM-300(In)-t and MFM-300(In)-e show typical features for In^{3+} at the surface as characterized by X-ray photoelectron spectroscopy (XPS) (Figure S6 and Table S1).

Electrochemical Reduction of CO_2. Carbon paper (CP) has a very coarse surface that can support materials to fabricate electrodes. Samples of MFM-300(In)-t and MFM-300(In)-e were loaded onto CP substrates using Nafion D-521 as a binder to fabricate MFM-300(In)-t/CP and MFM-300(In)-e/CP electrodes, respectively. Indium foil has a very smooth surface, and we were thus unable to fabricate MFM-300(In)-t/In since loading thermally prepared MFM-300(In)-t onto this metal surface was unsuccessful. The surface structures of MFM-300(In)-e/In, MFM-300(In)-t/CP and MFM-300(In)-e/CP were characterized by XPS (Figure S7 and Table S1). These spectra show typical features of In^{3+} cations, and the shifts in binding energy [+0.5 and −0.5 eV for MFM-300(In)-t and MFM-300(In)-e, respectively] compared to powder samples originate from the different conductivities of the surface substrates.

All three electrodes were investigated for electrochemical reduction of CO_2 in an H-type cell (Figure S8) with 0.5 M $EmimBF_4$ (1-ethyl-3-methylimidazolium tetrafluoroborate) in MeCN and 0.5 M H_2SO_4 as catholyte and anolyte, respectively. Cyclic voltammetry (CV) of MFM-300(In)-e/In was studied as a function of gas loading (Figure 3a). Large current densities were generated in the CO_2-saturated electrolyte, while negligible densities were observed for the electrolyte saturated with N_2. Controlled potential electrolysis at −2.0∼−2.3 V vs Ag/Ag^+ was conducted at room temperature under a flow of CO_2 into the electrolyte. All liquid and gas-phase products were quantified by ^1H NMR spectroscopy and gas chromatography (GC), respectively. Interestingly, only H_2 was observed in the gas phase and formic acid was identified as the sole product in the liquid phase. The electrolysis was performed for 2 h and results are summarized in Figure 3b, 3c. The current density increases with increasing applied potential in all cases and the Faradaic efficiency for formic acid (FE_{HCOOH}) reaches 99.1% with a current density of 46.1 mA cm^{-2} at −2.15 V vs Ag/Ag^+ for MFM-300(In)-e/In. Significantly, MFM-300(In)-e/In shows a higher current density compared with MFM-300(In)-e/CP and MFM-300(In)-t/CP at −2.15 V vs Ag/Ag^+; the latter gives the lowest FE_{HCOOH} at all potentials. The Faradaic efficiency for hydrogen (FE_{H2}) has an inverse trend over these electrodes (Figure S9) with MFM-300(In)-t/CP higher than MFM-300(In)-e/CP, which is higher than MFM-300(In)-e/In. In-foil, as a smooth metallic electrode (Figure S10), exhibits a current density of 19.7 mA cm^{-2} and FE_{HCOOH} of 50.7% in 0.5 M $EmimBF_4$/MeCN at −2.15 V vs Ag/Ag^+, lower than that

https://dx.doi.org/10.1021/jacs.0c05913
J. Am. Chem. Soc. 2020, 142, 17384−17392

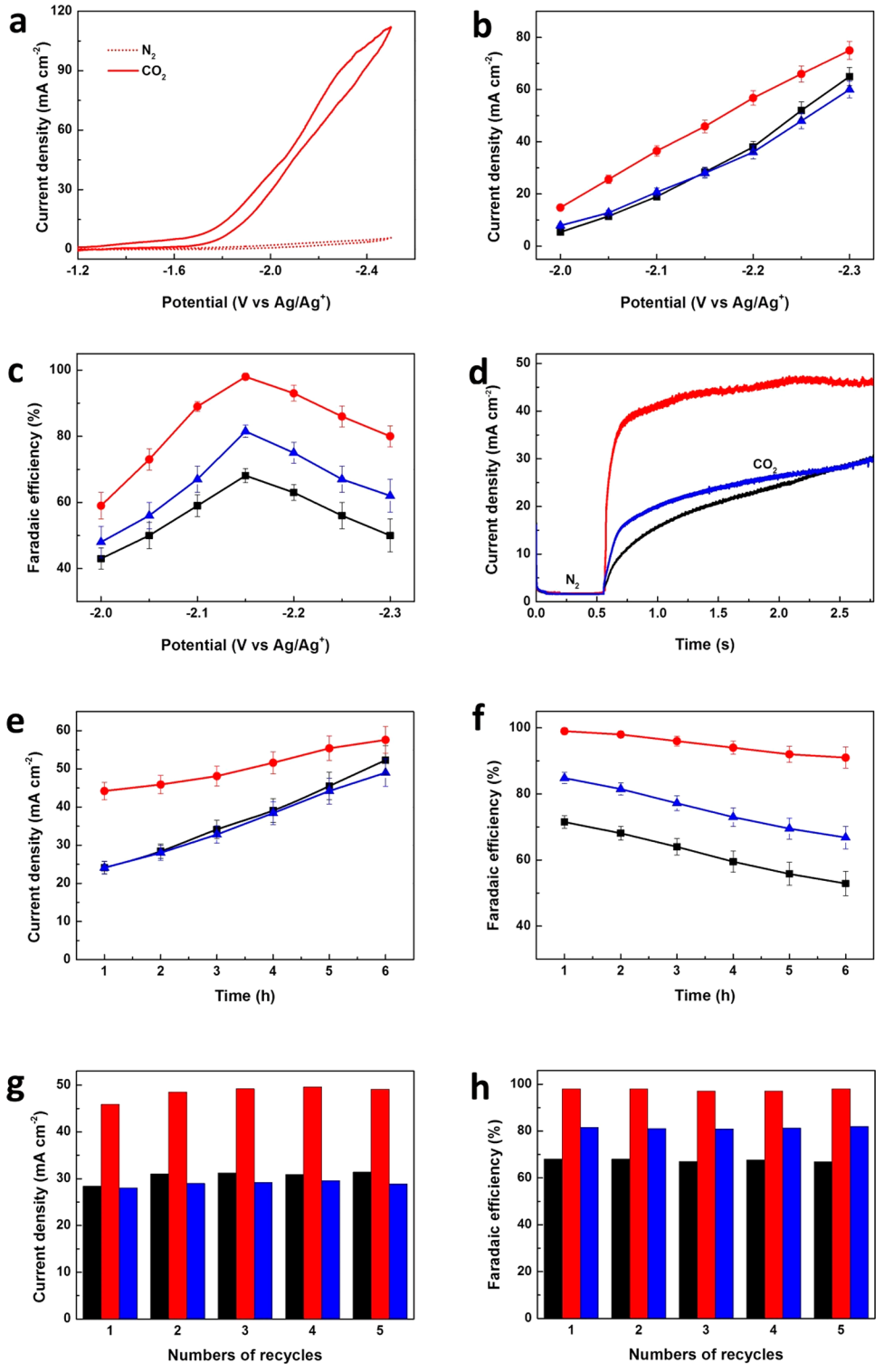

Figure 3. Electrochemical reduction of CO_2 over MFM-300(In)-t/CP (black), MFM-300(In)-e/In (red), and MFM-300(In)-e/CP (blue) in 0.5 M $EmimBF_4$/MeCN. (a) CV of MFM-300(In)-e/In in N_2- and CO_2-saturated electrolytes. (b) Plots of current density vs applied potential. (c) Plots of FE_{HCOOH} vs applied potential. (d) Plots of current density vs time before and after the introduction of CO_2. (e) Plots of current density vs time at −2.15 V vs Ag/Ag^+. (f) Plots of FE_{HCOOH} vs time at −2.15 V vs Ag/Ag^+. (g) Current density for five cycles of electrolysis at −2.15 V vs Ag/Ag^+ over 2 h. (h) FE_{HCOOH} for five cycles of electrolysis at −2.15 V vs Ag/Ag^+ over 2 h.

observed for MFM-300(In)-e/In under the same conditions (Table 1).

The dependence of current density and FE_{HCOOH} on time was studied further (Figure 3d). N_2 was first charged into the electrolyte, and an imperceptible current density was observed for all electrodes investigated. Significant increases in current density were observed over all electrodes on charging CO_2 into the electrolyte, with MFM-300(In)-e/In showing the strongest response to CO_2 and reaching a maximum current density most rapidly. No obvious inflection point was observed for the

https://dx.doi.org/10.1021/jacs.0c05913
J. Am. Chem. Soc. 2020, 142, 17384−17392

Table 1. Catalytic Performance for Electrochemical Reduction of CO_2 to Formic Acid Using Different Cathodes in the Organic Electrolyte

electrode	electrolyte	potential (V vs Ag/Ag^+)	j (mA cm^{-2})	FE_{HCOOH} (%)	ref
MFM-300(In)-e/In	0.5 M $EmimBF_4$/MeCN	−2.15	46.1	99.1	this work
MFM-300(In)-t/CP	0.5 M $EmimBF_4$/MeCN	−2.15	28.4	68.1	this work
MFM-300(In)-e/CP	0.5 M $EmimBF_4$/MeCN	−2.15	28.0	81.5	this work
In-foil	0.5 M $EmimBF_4$/MeCN	−2.15	19.7	50.7	this work
MoP@In-PC	$BmimPF_6$/MeCN/H_2O (30/65/5)	−2.2	43.8	96.5	43
Pb	700 mM BmimTrizu/MeCN/5 wt %H_2O	−2.4	24.5	95.2	44
Pb	$BmimPF_6$/MeCN/H_2O (30/65/5)	−2.2	17.8	95.3	45
Sn	$BmimPF_6$/MeCN/H_2O (30/65/5)	−2.2	15.8	95.0	45
Pb-PhyA	$BzmimBF_4$/MeCN/H_2O (12.8/77.3/9.9)	−2.25	30.5	92.7	46
SnO_2@N-PC	0.5 M $BmimPF_6$/MeCN	−2.2	28.4	94.1	47
Bi	250 mM (DBU-H)PF_6/acetonitrile/0.1 M $TBAPF_6$	−1.95[a]	27	77	56
Sn powder	0.5 M $EmimN(CN)_2$/H_2O	−1.2[b]	0.633	81.9	57

[a]vs SCE. [b]vs RHE.

MFM-300(In)-t/CP electrode, indicating that H_2 evolution occurred initially, accompanied by CO_2 reduction throughout. The electro-reduction of CO_2 was conducted for 6 h at −2.15 V vs Ag/Ag^+ to assess the long-term electrochemical stability of the electrodes (Figure 3e, 3f). After 6 h of electrolysis, the current density of MFM-300(In)-e/In had increased slowly to 57.6 mA cm^{-2} with a slightly decrease in FE_{HCOOH} to 91.2%. The average rate of production of formic acid is estimated to be 46 mg cm^{-2} h^{-1} for MFM-300(In)-e/In under these conditions (Figure S11). In contrast, the current density increased rapidly for MFM-300(In)-t/CP from 24.1 mA cm^{-2} (1 h) to 52.3 mA cm^{-2} (6 h) and for MFM-300(In)-e/CP from 24.1 mA cm^{-2} (1 h) to 49.0 mA cm^{-2} (6 h) but with notable decreases in FE_{HCOOH} to 52.9% and 66.8%, respectively. No carbon-containing product was detected in the gas phase product. The increased current density is assigned to H_2 evolution over the extended period of electrolysis, but MFM-300(In)-e/In retains a high selectivity toward the activation of CO_2 vs H_2 evolution (Figure S12). A comparison of the electrolytic performance for the formation of formic acid for MFM-300(In)-based electrodes and other state-of-the-art electrodes in organic electrolytes is given in Table 1, with MFM-300(In)-e/In showing the best performance.[43−47]

Reusability of Electrodes. All three electrodes were reused over five cycles for electro-reduction of CO_2 (Figure 3g,h). Both the current density and Faradaic efficiency for formation of formic acid show excellent stability for all three electrodes. During the electrolysis over MFM-300(In)-e/In, the surface of the electrode is rendered flat as confirmed by SEM (Figures 1d and S13). PXRD studies confirm retention of the structure of MFM-300(In)-e in cycled samples after electrolysis (Figure S14). XPS was used to study the surface properties of used MFM-300(In)-t/CP and MFM-300(In)-e/In electrodes (Figure S15). During the electrolysis, both MFM-300(In)-t/CP and MFM-300(In)-e/In electrodes evolved and the change of surface structure was accompanied by shifts of the In 3d peak (−0.5 eV and +0.5 eV, respectively), moving to the energy of the as-prepared MOF sample (Table S1). Before the electrolysis, MOF particles are relatively isolated (Figure 1d), and intercrystallite charge-transfer is thus restricted, resulting in the difference observed in XPS spectra. As the MOF surface evolves during the electrolysis, the surface becomes flatter and increasingly uniform (Figure S13), and the energy difference is therefore minimized. The absence of In^0 at the electrode surface suggests that In^{3+} sites in MFM-300(In) are not reduced during electrolysis,[48] consistent with the excellent electrochemical stability of MFM-300(In)-e/In.

Mechanistic Studies. Density functional theory (DFT) calculations afford the Gibbs free energy for the electro-reduction of CO_2 to formic acid over the pristine and defective MFM-300(In), representing MFM-300(In)-t and MFM-300(In)-e, respectively (Figure 4a). The formation of *COOH over pristine MFM-300(In) (* indicates an adsorption site on the MOF) involves a high energy barrier, indicating that this process is the rate-determining step. In contrast, the formation of *COOH is spontaneous over defective MFM-300(In)-e. The In^{3+} defects promote the adsorption of intermediate species, and therefore, higher Gibbs free energies are required for the desorption of *COOH and *HCOOH. The calculated reaction pathway of the electro-reduction of CO_2 over defective MFM-300(In) is shown in Figure S16. Furthermore, the Gibbs free energy for the formation of *COOH over In_2O_3, a benchmark indium-based catalyst, is very high (Figure S17), indicating that defective MFM-300(In) is a better candidate for the electro-reduction of CO_2. The adsorbed *COOH intermediate could be further reduced to *HCOOH or *CO.[10] The calculation of Gibbs free energy of electro-reduction of CO_2 to CO over defective MFM-300(In) has also been conducted, and we find that the *HCOOH intermediate is more readily formed than *CO due to the lower energy barrier for the former. This rationalizes the formation of formic acid as the main product over MFM-300(In)-based electrodes.

We have used 5,5-dimethyl-1-pyrroline *N*-oxide (DMPO)[49] as a spin trap to identify any radical species involved in the catalytic reaction. Figure 4b shows the EPR spectra of the reaction solution measured after electrolysis at −2.15 V vs Ag/Ag^+ using the different decorated electrodes. The EPR spectrum after electrolysis using MFM-300(In)-e/In shows three sets of radicals (Figure S19): two weak signals are assigned to oxidized DMPO radical ·DMPO-OX, a_N = 1.5 mT, and to ·DMPO−OH radicals, a_N = 1.43 mT, a_H = 1.33 mT.[50−52] Based upon established pathways for CO_2 reduction, ·DMPO−COOH radicals are the intermediate products (Figure S16).[53,54] In the above electrolysis we observe the formation of ·COOH with a_H = 2.21 mT.[52] The EPR spectra for the electrolysis reactions using MFM-300(In)-t/CP and MFM-300(In)-e/CP electrodes and their simulations are shown in Figures S20 and S21. The concentration

https://dx.doi.org/10.1021/jacs.0c05913
J. Am. Chem. Soc. 2020, 142, 17384−17392

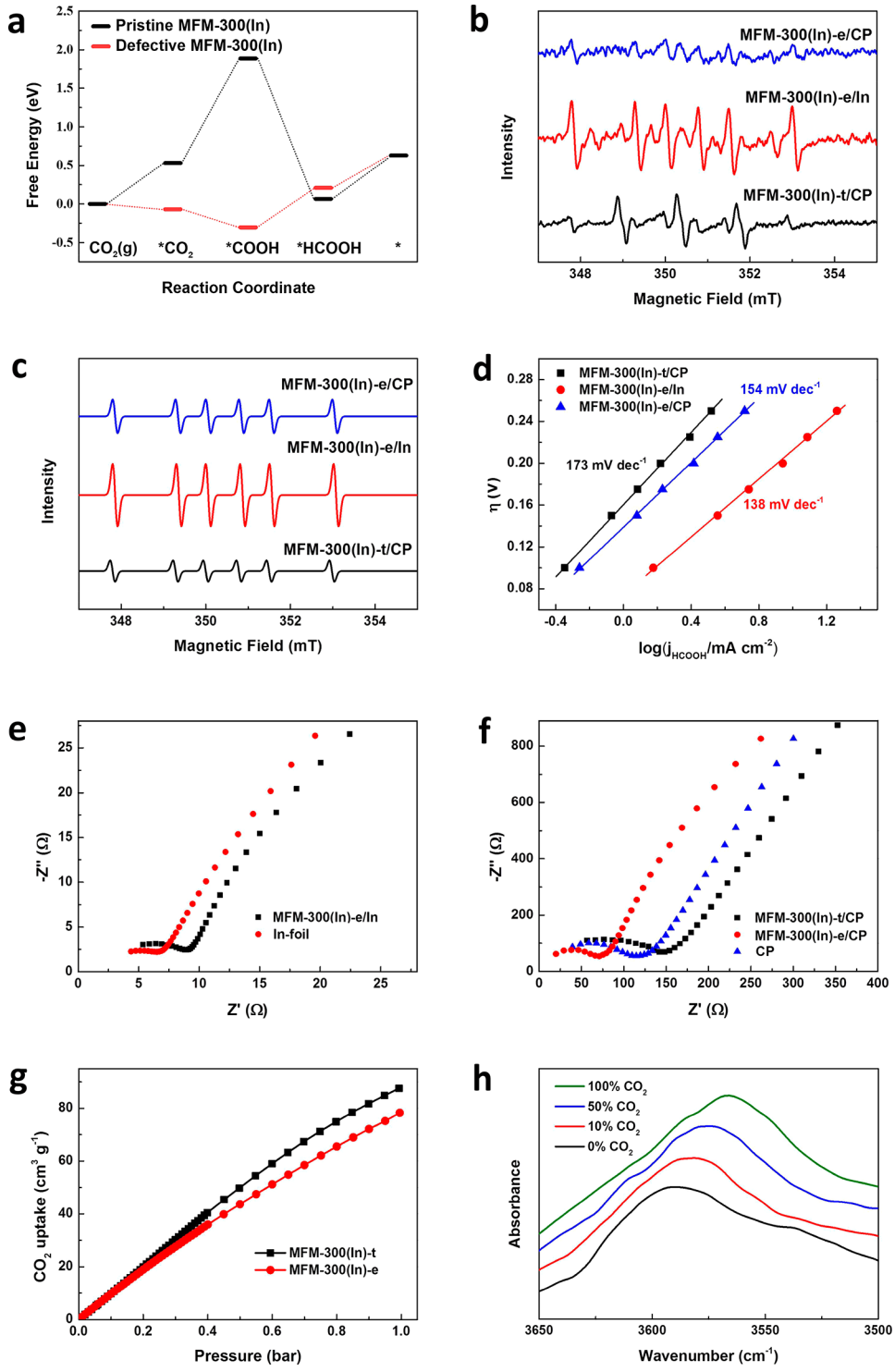

Figure 4. (a) Gibbs free energy profile derived from DFT calculations for electro-reduction of CO_2 to formic acid over pristine MFM-300(In) and defective MFM-300(In) (* indicates an adsorption site on the MOF). (b) EPR spectra of spin adducts of radicals formed during the electro-reduction of CO_2 using the three electrodes (0.5 M $EmimBF_4$/MeCN). (c) Comparison of ·DMPO−COOH radicals generated at different electrodes. (d) Tafel plots using different electrodes in this study. (e) Nyquist plots for electrodes using indium foil as substrate. (f) Nyquist plots for electrodes using CP as substrates. (g) Adsorption isotherms for CO_2 in MFM-300(In)-t and MFM-300(In)-e at 298 K. (h) In situ FTIR spectra of MFM-300(In)-e as a function of CO_2 loading.

of ·DMPO−COOH radicals in solution using MFM-300(In)-e/In is notably higher than in reactions at the MFM-300(In)-t/CP and MFM-300(In)-t/CP electrodes under the same conditions, consistent with the higher activity of MFM-300(In)-e/In (Figure 4c).

The Tafel plot is an indicator of the reaction pathway with the ease of reduction reflected in a lower overpotential.[8] The Tafel slope for reduction of CO_2 at MFM-300(In)-e/In, MFM-300(In)-t/CP and MFM-300(In)-e/CP electrodes are 138, 173, and 154 mV dec^{-1}, respectively (Figure 4d),

https://dx.doi.org/10.1021/jacs.0c05913
J. Am. Chem. Soc. 2020, 142, 17384−17392

indicating that the initial electron-transfer to generate surface-adsorbed $CO_2^{\bullet-}$ species is the rate-determining step.[12] Electrolysis using the MFM-300(In)-e/In electrode gives the lowest slope for the Tafel plot, indicating a higher absolute current density for a given overpotential compared with the other two electrodes. The MFM-300(In)-e/In electrode also shows more rapid kinetics for generation of radicals, consistent with the higher current density and higher FE_{HCOOH} for the electrolysis.

Electrochemical impedance spectroscopy (EIS) was conducted to investigate the properties of the electrode/electrolyte interface (Figures 4e, 4f).[43] Values for the interfacial charge-transfer resistance (R_{ct}) were obtained by fitting the experimental impedance data using Randles' equivalent circuit (Figure S22). The interface between MOF particles and the substrate is a significant barrier to charge transfer. The electro-synthesized MOF on In-foil gives a better interfacial contact, resulting in a lower R_{ct} for MFM-300(In)-e/In (9.5 Ω cm^2) compared with MFM-300(In)-e/CP (74.1 Ω cm^2). The lower R_{ct} for MFM-300(In)-e/CP (74.1 Ω cm^2) compared to MFM-300(In)-t/CP (178.2 Ω cm^2) is consistent with the presence of In^{3+} defect sites, which enhances the charge transfer of the former electrode. The higher double-layer capacitance value of MFM-300(In)-e/In (1.06 mF cm^{-2}) compared with MFM-300(In)-t/CP (0.31 mF cm^{-2}) and MFM-300(In)-e/CP (0.46 mF cm^{-2}), as measured by CV curves at −0.6 to −0.65 V vs Ag/Ag^+ at different scan rate (Figure S23), indicates that MFM-300(In)-e/In has higher electrochemical surface area.[19]

CO_2 adsorption isotherms of desolvated MFM-300(In)-t and MFM-300(In)-e show uptakes of 87.6 and 78.3 cm^3 g^{-1}, respectively, at 1 bar and 298 K (Figure 4g). The isosteric heat (Q_{st}) and entropies (ΔS) of adsorption (Figure S24) were determined by fitting of the Van't Hoff isochore from the adsorption isotherms of CO_2 at different temperatures (Figure S25). The value of Q_{st} of MFM-300(In)-e is higher than that of MFM-300(In)-t suggesting a stronger interaction of CO_2 with MFM-300(In)-e.

Synchrotron FTIR microspectroscopy of MFM-300(In)-e was recorded as a function of CO_2 loading at 298 K (Figure 4h). The change in the stretching mode $\nu(\mu_2\text{–OH})$ at 3600 cm^{-1} in the presence of CO_2 can provide direct insights into the strength of the host–guest binding. MFM-300(In)-t exhibits a red-shift of 5 cm^{-1} of the $\nu(\mu_2\text{–OH})$ stretching band on binding of CO_2.[55] In contrast, a red-shift of 25 cm^{-1} is observed for this stretching vibration on CO_2-loading into MFM-300(In)-e under the same conditions, suggesting that MFM-300(In)-e interacts more strongly with CO_2. This is consistent with the DFT calculation and Q_{st} analysis.

CONCLUSIONS

We have described a simple and effective strategy to prepare MOF-based electrodes via rapid electro-synthesis template by an ionic liquid. The as-prepared MFM-300(In)-e/In electrode incorporates active defect In^{3+} sites and shows high capacity for charge transfer and high electrochemical stability. This decorated electrode catalyzes the electro-reduction of CO_2 to formic acid with a current density of 46.1 mA cm^{-2} and a Faradaic efficiency, FE_{HCOOH} of 99.1% in organic electrolyte. To the best of our knowledge, this performance exceeds all other MOF systems. Overall, the excess In^{3+} sites in MFM-300(In)-e combined with a strong contact between the MOF and the indium foil leads to reduction in interfacial resistance resulting in exceptional activity, selectivity and stability for the electro-reduction of CO_2.

ASSOCIATED CONTENT

Supporting Information

The Supporting Information is available free of charge at https://pubs.acs.org/doi/10.1021/jacs.0c05913.

Additional experimental details, results, Figures S1-S25, and Table S1 (PDF)

AUTHOR INFORMATION

Corresponding Authors

Buxing Han − *Beijing National Laboratory for Molecular Sciences, CAS Key Laboratory of Colloid, Interface and Chemical Thermodynamics, Institute of Chemistry, Chinese Academy of Sciences, Beijing 100190, China;* orcid.org/0000-0003-0440-809X; Email: hanbx@iccas.ac.cn

Sihai Yang − *Department of Chemistry, The University of Manchester, Manchester M13 9PL, United Kingdom;* orcid.org/0000-0002-1111-9272; Email: Sihai.Yang@manchester.ac.uk

Martin Schröder − *Department of Chemistry, The University of Manchester, Manchester M13 9PL, United Kingdom;* orcid.org/0000-0001-6992-0700; Email: M.Schroder@manchester.ac.uk

Authors

Xinchen Kang − *Department of Chemistry, The University of Manchester, Manchester M13 9PL, United Kingdom*

Bin Wang − *Department of Chemistry, The University of Manchester, Manchester M13 9PL, United Kingdom*

Kui Hu − *Department of Chemistry, The University of Manchester, Manchester M13 9PL, United Kingdom*

Kai Lyu − *Department of Chemistry, The University of Manchester, Manchester M13 9PL, United Kingdom*

Xue Han − *Department of Chemistry, The University of Manchester, Manchester M13 9PL, United Kingdom*

Ben F. Spencer − *Department of Materials, The University of Manchester, Manchester M13 9PL, United Kingdom;* orcid.org/0000-0002-1453-5327

Mark D. Frogley − *Diamond Light Source, Oxfordshire OX11 0DE, United Kingdom*

Floriana Tuna − *Department of Chemistry and Photon Science Institute, The University of Manchester, Manchester M13 9PL, United Kingdom*

Eric J. L. McInnes − *Department of Chemistry, The University of Manchester, Manchester M13 9PL, United Kingdom;* orcid.org/0000-0002-4090-7040

Robert A. W. Dryfe − *Department of Chemistry, The University of Manchester, Manchester M13 9PL, United Kingdom*

Complete contact information is available at: https://pubs.acs.org/10.1021/jacs.0c05913

Notes

The authors declare no competing financial interest.

ACKNOWLEDGMENTS

We thank EPSRC (EP/I011870), the Royal Society (IC170327), National Natural Science Foundation of China (21733011 and 21890761), University of Manchester and Institute of Chemistry, Chinese Academy of Sciences for funding, and EPSRC for funding of the EPSRC National EPR

Facility at Manchester. This project has received funding from the European Research Council (ERC) under the European Union's Horizon 2020 research and innovation programme (Grant Agreement No. 742401, NANOCHEM). X.K. is supported by a Royal Society Newton International Fellowship. We are grateful to Diamond Light Source for access to the Beamline B22. K.H. and K.L. acknowledge the China Scholarship Council for funding.

REFERENCES

(1) Diercks, C. S.; Liu, Y. Z.; Cordova, K. E.; Yaghi, O. M. The Role of Reticular Chemistry in the Design of CO_2 Reduction Catalysts. *Nat. Mater.* **2018**, *17*, 301−307.
(2) Voiry, D.; Shin, H. S.; Loh, K. P.; Chhowalla, M. Low-Dimensional Catalysts for Hydrogen Evolution and CO_2 Reduction. *Nat. Rev. Chem.* **2018**, *2*, 0105.
(3) Li, X.; Yu, J. G.; Jaroniec, M.; Chen, X. B. Cocatalysts for Selective Photoreduction of CO_2 into Solar Fuels. *Chem. Rev.* **2019**, *119*, 3962−4179.
(4) An, B.; Zhang, J. Z.; Cheng, K.; Ji, P. F.; Wang, C.; Lin, W. B. Confinement of Ultrasmall Cu/ZnO_x Nanoparticles in Metal-Organic Frameworks for Selective Methanol Synthesis from Catalytic Hydrogenation of CO_2. *J. Am. Chem. Soc.* **2017**, *139*, 3834−3840.
(5) Kattel, S.; Ramírez, P. J.; Chen, J. G.; Rodriguez, J. A.; Liu, P. Active Sites for CO_2 Hydrogenation to Methanol on Cu/ZnO Catalysts. *Science* **2017**, *355*, 1296−1299.
(6) Dong, C. Y.; Lian, C.; Hu, S. C.; Deng, Z. S.; Gong, J. Q.; Li, M. D.; Liu, H. L.; Xing, M. Y.; Zhang, J. L. Size-Dependent Activity and Selectivity of Carbon Dioxide Photocatalytic Reduction over Platinum Nanoparticles. *Nat. Commun.* **2018**, *9*, 1252.
(7) Yu, H. J.; Li, J. Y.; Zhang, Y. H.; Yang, S. Q.; Han, K. L.; Dong, F.; Ma, T. Y.; Huang, H. W. Three-in-One Oxygen Vacancies: Whole Visible-Spectrum Absorption, Efficient Charge Separation, and Surface Site Activation for Robust CO_2 Photoreduction. *Angew. Chem., Int. Ed.* **2019**, *58*, 3880−3884.
(8) Zhang, L.; Zhao, Z. J.; Gong, J. L. Nanostructured Materials for Heterogeneous Electrocatalytic CO_2 Reduction and their Related Reaction Mechanisms. *Angew. Chem., Int. Ed.* **2017**, *56*, 11326−11353.
(9) Jin, H. Y.; Guo, C. X.; Liu, X.; Liu, J. L.; Vasileff, A.; Jiao, Y.; Zheng, Y.; Qiao, S. Z. Emerging Two-Dimensional Nanomaterials for Electrocatalysis. *Chem. Rev.* **2018**, *118*, 6337−6408.
(10) Zhu, D. D.; Liu, J. L.; Qiao, S. Z. Recent Advances in Inorganic Heterogeneous Electrocatalysts for Reduction of Carbon Dioxide. *Adv. Mater.* **2016**, *28*, 3423−3452.
(11) Zhu, H. J.; Lu, M.; Wang, Y. R.; Yao, S. J.; Zhang, M.; Kan, Y. H.; Liu, J.; Chen, Y. F.; Li, S. L.; Lan, Y. Q. Efficient Electron Transmission in Covalent Organic Framework Nanosheets for Highly Active Electrocatalytic Carbon Dioxide Reduction. *Nat. Commun.* **2020**, *11*, 497.
(12) Gu, J.; Hsu, C. S.; Bai, L. C.; Chen, H. M.; Hu, X. L. Atomically Dispersed Fe^{3+} Sites Catalyze Efficient CO_2 Electroreduction to CO. *Science* **2019**, *364*, 1091−1094.
(13) Zheng, X. L.; Ji, Y. F.; Tang, J.; Wang, J. Y.; Liu, B. F.; Steinruck, H. G.; Lim, K.; Li, Y. Z.; Toney, M. F.; Chan, K.; Cui, Y. Theory-Guided Sn/Cu Alloying for Efficient CO_2 Electroreduction at Low Overpotentials. *Nat. Catal.* **2019**, *2*, 55−61.
(14) Pang, Y.; Li, J.; Wang, Z.; Tan, C.-S.; Hsieh, P.-L.; Zhuang, T.-T.; Liang, Z.-Q.; Zou, C.; Wang, X.; De Luna, P.; Edwards, J. P.; Xu, Y.; Li, F.; Dinh, C.-T.; Zhong, M.; Lou, Y.; Wu, D.; Chen, L.-J.; Sargent, E. H.; Sinton, D. Efficient Electrocatalytic Conversion of Carbon Monoxide to Propanol Using Fragmented Copper. *Nat. Catal.* **2019**, *2*, 251−258.
(15) Wang, Y. R.; Huang, Q.; He, C. T.; Chen, Y. F.; Liu, J.; Shen, F. C.; Lan, Y. Q. Oriented Electron Transmission in Polyoxometalate-Metalloporphyrin Organic Framework for Highly Selective Electroreduction of CO_2. *Nat. Commun.* **2018**, *9*, 4466.
(16) Gao, S.; Lin, Y.; Jiao, X. C.; Sun, Y. F.; Luo, Q. Q.; Zhang, W. H.; Li, D. Q.; Yang, J. L.; Xie, Y. Partially Oxidized Atomic Cobalt Layers for Carbon Dioxide Electroreduction to Liquid Fuel. *Nature* **2016**, *529*, 68−71.
(17) Kwak, K.; Lee, D. Electrochemistry of Atomically Precise Metal Nanoclusters. *Acc. Chem. Res.* **2019**, *52*, 12−22.
(18) Li, J.; Wang, X. X.; Zhao, G. X.; Chen, C. L.; Chai, Z. F.; Alsaedi, A.; Hayat, T.; Wang, X. K. Metal-Organic Framework-Based Materials: Superior Adsorbents for the Capture of Toxic and Radioactive Metal Ions. *Chem. Soc. Rev.* **2018**, *47*, 2322−2356.
(19) Yang, Q. H.; Xu, Q.; Jiang, H. L. Metal-Organic Frameworks Meet Metal Nanoparticles: Synergistic Effect for Enhanced Catalysis. *Chem. Soc. Rev.* **2017**, *46*, 4774−480.
(20) Yu, J. M.; Xie, L. H.; Li, J. R.; Ma, Y. G.; Seminario, J. M.; Balbuena, P. B. CO_2 Capture and Separations Using MOFs: Computational and Experimental Studies. *Chem. Rev.* **2017**, *117*, 9674−9754.
(21) Kang, X. C.; Zhu, Q. G.; Sun, X. F.; Hu, J. Y.; Zhang, J. L.; Liu, Z. M.; Han, B. X. Highly Efficient Electrochemical Reduction of CO_2 to CH_4 in an Ionic Liquid Using a Metal-Organic Framework Cathode. *Chem. Sci.* **2016**, *7*, 266−273.
(22) Kornienko, N.; Zhao, Y.; Kley, C. S.; Zhu, C.; Kim, D.; Lin, S.; Chang, C. J.; Yaghi, O. M.; Yang, P. Metal-Organic Frameworks for Electrocatalytic Reduction of Carbon Dioxide. *J. Am. Chem. Soc.* **2015**, *137*, 14129−14135.
(23) Lin, S.; Diercks, C. S.; Zhang, Y. B.; Kornienko, N.; Nichols, E. M.; Zhao, Y. B.; Paris, A. R.; Kim, D.; Yang, P.; Yaghi, O. M.; Chang, C. J. Covalent Organic Frameworks Comprising Cobalt Porphyrins for Catalytic CO_2 Reduction in Water. *Science* **2015**, *349*, 1208−1213.
(24) Smith, P. T.; Benke, B. P.; Cao, Z.; Kim, Y.; Nichols, E. M.; Kim, K.; Chang, C. J. Iron Porphyrins Embedded into a Supramolecular Porous Organic Cage for Electrochemical CO_2 Reduction in Water. *Angew. Chem., Int. Ed.* **2018**, *57*, 9684−9688.
(25) Weng, Z.; Wu, Y. S.; Wang, M. Y.; Jiang, J. B.; Yang, K.; Huo, S. J.; Wang, X. F.; Ma, Q.; Brudvig, G. W.; Batista, V. S.; Liang, Y. Y.; Feng, Z. X.; Wang, H. L. Active Sites of Copper-Complex Catalytic Materials for Electrochemical Carbon Dioxide Reduction. *Nat. Commun.* **2018**, *9*, 415.
(26) Yang, H. B.; Hung, S. F.; Liu, S.; Yuan, K. D.; Miao, S.; Zhang, L. P.; Huang, X.; Wang, H. Y.; Cai, W. Z.; Chen, R.; Gao, J. J.; Yang, X. F.; Chen, W.; Huang, Y. Q.; Chen, H. M.; Li, C. M.; Zhang, T.; Liu, B. Atomically Dispersed Ni(I) as the Active Site for Electrochemical CO_2 Reduction. *Nat. Energy* **2018**, *3*, 140−147.
(27) Chaemchuen, S.; Kabir, N. A.; Zhou, K.; Verpoort, F. Metal-Organic Frameworks for Upgrading Biogas *Via* CO_2 Adsorption to Biogas Green Energy. *Chem. Soc. Rev.* **2013**, *42*, 9304−9332.
(28) Park, J.; Yuan, D. Q.; Pham, K. T.; Li, J. R.; Yakovenko, A.; Zhou, H. C. Reversible Alteration of CO_2 Adsorption upon Photochemical or Thermal Treatment in a Metal-Organic Framework. *J. Am. Chem. Soc.* **2012**, *134*, 99−102.
(29) Huang, Q.; Li, Q.; Liu, J.; Wang, Y. R.; Wang, R.; Dong, L. Z.; Xia, Y. H.; Wang, J. L.; Lan, Y. Q. Disclosing CO_2 Activation Mechanism by Hydroxyl-Induced Crystalline Structure Transformation in Electrocatalytic Process. *Matter* **2019**, *1*, 1656−1668.
(30) Hod, I.; Bury, W.; Karlin, D. M.; Deria, P.; Kung, C. W.; Katz, M. J.; So, M.; Klahr, B.; Jin, D. N.; Chung, Y. W.; Odom, T. W.; Farha, O. K.; Hupp, J. T. Directed Growth of Electroactive Metal-Organic Framework Thin Films Using Electrophoretic Deposition. *Adv. Mater.* **2014**, *26*, 6295−6300.
(31) Hauser, J. L.; Tso, M.; Fitchmun, K.; Oliver, S. R. J. Anodic Electrodeposition of Several Metal Organic Framework Thin Films on Indium Tin Oxide Glass. *Cryst. Growth Des.* **2019**, *19*, 2358−2365.
(32) Li, M. Y.; Dincă, M. Selective Formation of Biphasic Thin Films of Metal-Organic Frameworks by Potential-Controlled Cathodic Electrodeposition. *Chem. Sci.* **2014**, *5*, 107−111.
(33) Antonio, A. M.; Rosenthal, J.; Bloch, E. D. Electrochemically Mediated Syntheses of Titanium(III)-Based Metal-Organic Frameworks. *J. Am. Chem. Soc.* **2019**, *141*, 11383−11387.

https://dx.doi.org/10.1021/jacs.0c05913
J. Am. Chem. Soc. 2020, 142, 17384−17392

(34) Dong, B. X.; Qian, S. L.; Bu, F. Y.; Wu, Y. C.; Feng, L. G.; Teng, Y. L.; Liu, W. L.; Li, Z. W. Electrochemical Reduction of CO_2 to CO by a Heterogeneous Catalyst of Fe-Porphyrin-Based Metal-Organic Framework. *ACS Appl. Energy Mate.* **2018**, *1*, 4662−4669.
(35) Bohlen, B.; Wastl, D.; Radomski, J.; Sieber, V.; Vieira, L. Electrochemical CO_2 Reduction to Formate on Indium Catalysts Prepared by Electrodeposition in Deep Eutectic Solvents. *Electrochem. Commun.* **2020**, *110*, 106597.
(36) Luo, W.; Xie, W.; Li, M.; Zhang, J.; Züttel, A. 3D Hierarchical Porous Indium Catalyst for Highly Efficient Electroreduction of CO_2. *J. Mater. Chem. A* **2019**, *7*, 4505−4515.
(37) Ameloot, R.; Stappers, L.; Fransaer, J.; Alaerts, L.; Sels, B. F.; De Vos, D. E. Patterned Growth of Metal-Organic Framework Coatings by Electrochemical Synthesis. *Chem. Mater.* **2009**, *21*, 2580−2582.
(38) Li, M. Y.; Dincă, M. Reductive Electrosynthesis of Crystalline Metal-Organic Frameworks. *J. Am. Chem. Soc.* **2011**, *133*, 12926−12929.
(39) Martinez Joaristi, A.; Juan-Alcañiz, J.; Serra-Crespo, P.; Kapteijn, F.; Gascon, J. Electrochemical Synthesis of Some Archetypical Zn^{2+}, Cu^{2+}, and Al^{3+} Metal Organic Frameworks. *Cryst. Growth Des.* **2012**, *12*, 3489−3498.
(40) Ji, H.; Hwang, S.; Kim, K.; Kim, C.; Jeong, N. C. Direct *in situ* Conversion of Metals into Metal-Organic Frameworks: A Strategy for the Rapid Growth of MOF Films on Metal Substrates. *ACS Appl. Mater. Interfaces* **2016**, *8*, 32414−32420.
(41) Qian, J. J.; Jiang, F. L.; Yuan, D. Q.; Wu, M. Y.; Zhang, S. Q.; Zhang, L. J.; Hong, M. C. Highly Selective Carbon Dioxide Adsorption in a Water-Stable Indium-Organic Framework Material. *Chem. Commun.* **2012**, *48*, 9696−9698.
(42) Sang, X. X.; Zhang, J. L.; Xiang, J. F.; Cui, J.; Zheng, L. R.; Zhang, J.; Wu, Z. H.; Li, Z. H.; Mo, G.; Xu, Y.; Song, J. L.; Liu, C. C.; Tan, X. N.; Luo, T.; Zhang, B. X.; Han, B. X. Ionic Liquid Accelerates the Crystallization of Zr-Based Metal-Organic Frameworks. *Nat. Commun.* **2017**, *8*, 175.
(43) Sun, X. F.; Lu, L.; Zhu, Q. G.; Wu, C. Y.; Yang, D. X.; Chen, C. J.; Han, B. X. MoP Nanoparticles Supported on Indium-Doped Porous Carbon: Outstanding Catalysts for Highly Efficient CO_2 Electroreduction. *Angew. Chem., Int. Ed.* **2018**, *57*, 2427−2431.
(44) Feng, J. P.; Zeng, S. J.; Liu, H. Z.; Feng, J. Q.; Gao, H. S.; Bai, L.; Dong, H. F.; Zhang, S. J.; Zhang, X. P. Insights into Carbon Dioxide Electroreduction in Ionic Liquids: Carbon Dioxide Activation and Selectivity Tailored by Ionic Micro-Habitat. *ChemSusChem* **2018**, *11*, 3191−3197.
(45) Zhu, Q. G.; Ma, J.; Kang, X. C.; Sun, X. F.; Liu, H. Z.; Hu, J. Y.; Liu, Z. M.; Han, B. X. Efficient Reduction of CO_2 into Formic Acid on a Lead or Tin Electrode Using an Ionic Liquid Catholyte Mixture. *Angew. Chem., Int. Ed.* **2016**, *55*, 9012−9016.
(46) Wu, H. R.; Song, J. L.; Xie, C.; Hu, Y.; Ma, J.; Qian, Q. L.; Han, B. X. Design of Naturally Derived Lead Phytate as an Electrocatalyst for Highly Efficient CO_2 Reduction to Formic Acid. *Green Chem.* **2018**, *20*, 4602−4606.
(47) Lu, L.; Sun, X. F.; Ma, J.; Zhu, Q. G.; Wu, C. Y.; Yang, D. X.; Han, B. X. Selective Electroreduction of Carbon Dioxide to Formic Acid on Electrodeposited SnO_2@N-Doped Porous Carbon Catalysts. *Sci. China: Chem.* **2018**, *61*, 228−235.
(48) Larrazábal, G. O.; Martín, A. J.; Mitchell, S.; Hauert, R.; Pérez-Ramirez, J. Enhanced Reduction of CO_2 to CO Over Cu-In Electrocatalysts: Catalyst Evolution Is the Key. *ACS Catal.* **2016**, *6*, 6265−6274.
(49) Villamena, F. A.; Locigno, E. J.; Rockenbauer, A.; Hadad, C. M.; Zweier, J. L. Theoretical and Experimental Studies of the Spin Trappingof Inorganic Radicals by 5,5-Dimethyl-1-Pyrroline N-Oxide (DMPO). 1. Carbon Dioxide Radical Anion. *J. Phys. Chem. A* **2006**, *110*, 13253−13258.
(50) Feng, G. D.; Cheng, P.; Yan, W. F.; Boronat, M.; Li, X.; Su, J. H.; Wang, J. Y.; Li, Y.; Corma, A.; Xu, R. R.; Yu, J. H. Accelerated Crystallization of Zeolites Via Hydroxyl Free Radicals. *Science* **2016**, *351*, 1188−1191.
(51) Fontmorin, J.M.; Burgos Castillo, R.C.; Tang, W.Z.; Sillanpaa, M. Stability of 5,5-Dimethyl-1-Pyrroline-N-Oxide as a Spin-Trap for Quantification of Hydroxyl Radicals in Processes Based on Fenton Reaction. *Water Res.* **2016**, *99*, 24−32.
(52) Buettner, G. R. Spin Trapping: ESR Parameters of Spin Adducts. *Free Radical Biol. Med.* **1987**, *3*, 259−303.
(53) Feaster, J. T.; Shi, C.; Cave, E. R.; Hatsukade, T. T.; Abram, D. N.; Kuhl, K. P.; Hahn, C.; Norskøv, J. K.; Jaramillo, T. F. Understanding Selectivity for the Electrochemical Reduction of Carbon Dioxide to Formic Acid and Carbon Monoxide on Metal Electrodes. *ACS Catal.* **2017**, *7*, 4822−4827.
(54) Sun, Z. Y.; Ma, T.; Tao, H. C.; Fan, Q.; Han, B. X. Fundamentals and Challenges of Electrochemical CO_2 Reduction Using Two-Dimensional Materials. *Chem.* **2017**, *3*, 560−587.
(55) Savage, M.; Cheng, Y.; Easun, T. L.; Eyley, J. E.; Argent, S. P.; Warren, M. R.; Lewis, W.; Murray, C.; Tang, C. C.; Frogley, M. D.; Cinque, G.; Sun, J.; Rudic, S.; Murden, R. T.; Benham, M. J.; Fitch, A. N.; Blake, A. J.; Ramirez-Cuesta, A. J.; Yang, S.; Schroder, M. Selective Adsorption of Sulfur Dioxide in a Robust Metal-Organic Framework Material. *Adv. Mater.* **2016**, *28*, 8705−8711.
(56) Atifi, A.; Boyce, D. W.; DiMeglio, J. L.; Rosenthal, J. Directing the Outcome of CO_2 Reduction at Bismuth Cathodes Using Varied Ionic Liquid Promoters. *ACS Catal.* **2018**, *8*, 2857−2863.
(57) Zhang, X.; Zhao, Y.; Hu, S.; Gliege, M. E.; Liu, Y.; Liu, R.; Scudiero, L.; Hu, Y.; Ha, S. Electrochemical Reduction of Carbon Dioxide to Formic Acid in Ionic Liquid $[Emim][N(CN)_2]$/Water System. *Electrochim. Acta* **2017**, *247*, 281−287.

https://dx.doi.org/10.1021/jacs.0c05913
J. Am. Chem. Soc. 2020, 142, 17384−17392